A large-scale-oriented growth of ZnO nanorod array on glass substrate: growth, structural and photoluminoscent properties

A. SANTHOSH KUMAR, H. S. NAGARAJA[*]
Materials Research Lab, Department of Physics, National Institute of Technology Karnataka, Surathkal-575025, India

We report a modified sol gel route for one step fabrication of large scale arrays of zinc oxide (ZnO) nanorods. The method is seed layer free, and nanorods are directly attached to a substrate. We studied the effect of PVA content on growth, crystallanity, orientation, microstructure and optical properties of ZnO. The XRD patterns confirm that samples grown with PVA have good crystallanity with (002) preferred orientation. The SEM micrographs show that the 1 Wt% PVA assisted grown films are covered with large scale oriented nanorod array. Raman spectrum represents that the 1 wt% PVA assisted grown ZnO nanostructures are highly crystalline with a hexagonal wurtzite phase. The room temperature PL spectrum exhibits a strong and sharp UV emission, which confirms that the grown arrays have good optical properties with few structural defects such as oxygen vacancies and zinc interstitials.

1. Introduction

In recent years, One-dimensional (1D) ZnO nanostructures, typically highly oriented and aligned ZnO nanorod arrays have received considerable research attention for the development of novel devices, such as room temperature UV-lasers, light emitting diodes, solar cells, gas sensors and so on [1-6]. Various physical and chemical methods have been developed for the fabrication of ZnO nanorod arrays, including pulsed laser deposition [5], vapor-liquid-solid (VLS) process [7], chemical vapor deposition (CVD) [8], metal organic vapor-phase epitaxy (MOVPE) [9], seed layer assisted hydrothermal route [10], electrochemical deposition [4,11] and sol gel process [12-14]. Compared with the physical vapor techniques, the solution based approaches exhibits obvious advantages in time, cost, complexity, energy consumption and large product yield. The growth of ZnO nanorod array has been demonstrated in several solution systems including zinc nitrate- HTMA [10,15,16]/sodium hydroxide [17]/ammonium hydroxide [18], zinc acetate-citric acid [19]. In order to achieve the vertical geometry of ZnO nanorods, either spin -coated ZnO layers [15], electrodeposited ZnO layers [16], sputtered ZnO films [17], evaporated Zn metal film [18] or zinc metal foil has been used as the substrate. When the pre deposited ZnO seed layer is absent, misaligned and randomly oriented ZnO nanorods can be obtained [20,21]. Inspiringly, several groups [14,21,22,23] realized the direct growth of ZnO nanorod arrays on substrates, but well aligned and oriented nanorods are not obtained in their studies. However, the direct growth of well aligned nanostructures with preferred orientation is an ultimate goal to meet various demands of practical applications. This notion leads us to explore a simple, catalyst-free, and seed-layer-free method for obtaining the well aligned with preferred orientation ZnO arrays. Thus, Polyvinyl alcohol (PVA)-Citric acid (CA) modified sol-gel approach for the growth of well aligned *c*-axis oriented ZnO nanorod arrays is desirable. In the present work, we synthesized successfully c-axis oriented well aligned ZnO nanorod arrays directly by PVA-CA assisted sol-gel technique without any pre-deposited seed layers. The alignment and orientation of nanorods from this method was studied by tailoring the PVA concentration.

2. Experimental details

2.1 Substrate cleaning

Commercially available glass slides with a size of 20 mm × 20 mm × 1 mm were washed using soap solution and subsequently kept in piranha solution for 6 hrs to remove the organic residues. Finally, the substrates were cleaned with deionized water followed by rinsing in acetone and stored in a hot oven.

2.2 Preparation of ZnO nanorod arrays

Polyvinyl alcohol (PVA) with molecular weight of 1,40,000 g/mol [Aldrich], zinc acetate dehydrate [Zn(CH$_3$COO)$_2$.2H$_2$O, Aldrich] and citric acid [Merck] were used as the precursors. The polymer gel for deposition was prepared by dissolving 0, 0.5, 1, 2 wt% of PVA in 50 ml distilled water and stirred at 80 °C for 8 h. 1M zinc acetate was added to the resulting solution, while stirring at 80°C. A clear homogeneous gel was obtained. The pH of above gel

solution is adjusted at 6.4 using citric acid. The gel solution was ultrasonicated at 80°C for 2 hrs and aged for 24 hr in order to make the PVA chains fully complex with the metal ions. Subsequently, ZnO polymer gel was two times spin coated onto the cleaned glass substrates. The intermediate drying between successive coatings was done at 180°C for 30 min. The prepared films were initially heat treated at 250°C for 60 min, to promote pyrolysis of the polymer resin, resulting in an amorphous film, and later crystallized by annealing at 450°C for 1h. The heating rate was kept at 2°C/min. The dried precursor and films were characterized and analyzed by different characterization techniques.

The decomposition of PVA was confirmed by TGA results. The crystallographic studies were performed using JEOL X-ray Diffractometer (JDX-8030) using Cu-Kα wavelength (λ=1.54059 Å) with scanning range from 10° to 50°. The surface morphology of the films was observed with JEOL scanning electron microscopy (JSM-6380 LV). The Raman spectra were measured on Alpha 300 WITec at room temperature using 532 nm laser. The photoluminescence spectra were recorded from 330 nm to 600 nm at room temperature by a 325 nm excitation from Xe lamp (F-4500 Fluorescence Spectrophotometer).

3. Results and discussion

3.1. Thermal analysis

The thermodecompostion behavior of the dried PVA -zinc acetate gel was studied by TGA and DTA analysis. Fig. 1 shows TG-DTA curves recorded on PVA -zinc acetate dried gel, which shows that most of the organic belonged to PVA and CH_3COO group of zinc acetate and other volatiles (H_2O, COx, etc.) were removed at temperature <500°C.
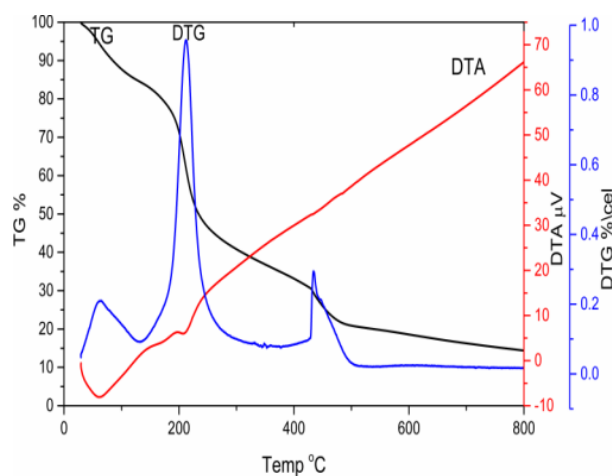

Fig. 1. TG-DTA and DTG curves recorded on 1 Wt% PVA –Zinc acetate dried gel precursor.

The TGA curve exhibits mainly three apparent weight losses. The first step of weight loss (21%) in the temperature range of 32°C to 135°C in TGA is accompanied by a small endothermic peak near 76.04°C in the DTA curve, which was caused by the loss of the surface absorbed water or the residual water molecules in the dried gel sample. The second step of weight loss (41%) was noticed between 135°C to 350°C which is accompanied by an exothermic peak near 230.43°C in the DTA curve, due to the decomposition of the acetate and side-chain of PVA. The last weight loss of 23% was observed from 350°C to 495°C. In the DTA curve, a wide exothermic peak was located at 445°C, which was likely to be due to the oxidation combustion of the PVA main chain. Above 500°C, the TG and DTA curves were all stable, indicating that water, organic compounds, chlorides and acetate in the dried gel sample were completely volatilized and pure ZnO nanosized particles could be obtained. There was only a weight loss of 5.0% from 435°C up to a temperature of 550°C, after which there was no change in weight loss, indicating that the formation of pure inorganic oxide. The total weight loss of 85% has been observed. Therefore, based on the TG-DTA curves the temperature of 450°C was selected as the calcination temperature in the procedure.
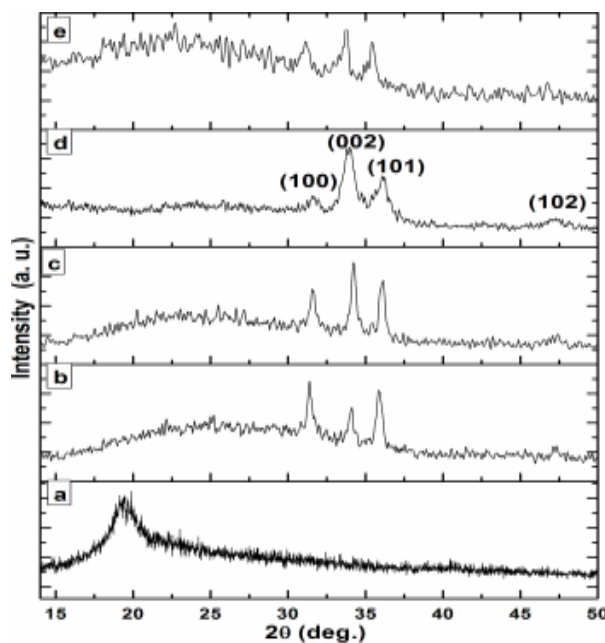
3.2. X – Ray Diffraction (XRD) studies

Fig. 2. XRD patterns of ZnO films prepared in presence of different PVA content (a) 1 Wt% at 180°C, (b) 0 Wt% at 450°C, (c) 0.5Wt% at 450°C, (d) 1Wt% at 450°C, (e) 2 Wt% at 450°C.

The results obtained by TG were confirmed by XRD measurements. X-ray diffraction pattern of ZnO films prepared using PVA-citric acid thermolysis assisted sol gel method is shown in Fig 2. In Fig. 2(a), a broad peak around 2θ=20° corresponds to the (101) plane of semi-crystalline PVA [24] in PVA-ZnO film dried at 180°C. This shows that

the crystallinity of PVA was largely influenced by the presence of zinc oxide, indicating an interaction between organic and amorphous zinc oxide fine particles. Notably, after the films are calcined at 450°C for 60 min, crystalline peak of PVA disappeared, XRD patterns revealed that all the films are polycrystalline ZnO with a wurtzite structure (Fig. 2 (b-e)).

Table 1. Bragg angle (2θ), Planes (hkl), Crystallite size (D), Lattice parameters (a & c), Texture coefficient(TC) evaluated from XRD pattern.

PVA content	2θ (deg.)	(hkl)	Crystallite size (D) nm	Texture coefficient (TC) (002)	Lattice Parameters (A°)
0	31.317 34.088 35.746	100 002 101	72	0.82	a=b= 3.116 c= 5.255
0.5	31.901 34.422 36.604	100 002 101	59	1.68	a=b= 3.173 c= 5.206
1	31.701 34.402 36.212	100 002 101	38	1.94	a=b= 3.160 c= 5.207
2	31.631 34.240 35.433	100 002 101	30	1.34	a=b= 3.146 c= 5.237

Three well defined diffraction planes are appeared at 31.7° (100), 34.4° (002), 36.2° (101) corresponding to pure ZnO (JCPDF: 075-0576; a=b= 3.2499 Å, c= 5.2066 Å) crystalline phase. No peaks corresponding to either carbon, zinc or any of its other oxides are observed in the XRD patterns, which indicate that there are no additional impurities phase present in ZnO films. The films grown with PVA show preferred orientation with c-axis perpendicular to the substrate. The (002) peak intensity is found to be high for the 1 Wt% PVA assisted grown sample at 450°C, indicating a better crystallinity as shown in Fig. 2(d). The intensity of the (002) peak shows a significant decrease with the further increase of PVA content to 2 Wt%. This indicates the decrease in crystallite size and crystallanity (Fig. 2(e)). The crystallite sizes of ZnO films have been estimated using Scherer's formula [25]. The grain size values of 0, 0.5, 1 and 2 Wt% PVA assisted grown ZnO films are given in Table 1. The preferential or random growth of polycrystalline thin films can be understood by calculating the texture coefficient TC (h k l) for all planes. The texture coefficient is calculated using the fallowing equation [25]

$$TC(hkl) = \frac{I(hkl) \big/ Io(hkl)}{\frac{1}{N} \sum I(hkl) \big/ Io(hkl)}$$

Where I(h k l) is the X-ray diffraction intensities obtained from the films, and N is the number of reflections observed in the XRD pattern. I_o(h k l) is the intensity of the standard diffraction pattern of JCPDS card 75-0576. It is clear from the definition that the deviation of texture coefficient from the unity implies the film growth occurs in certain preferred orientation. Table 1 shows the variation of the texture coefficient with PVA content for the (002) plane. The texture coefficients of (002) plane of the 0, 0.5, 1 and 2W% PVA assisted grown films are found to be 0.82, 1.68, 1.94 and 1.34, respectively. Without PVA assisted grown sample (Fig. 2(b)) has not shown (002) preferred orientation due to deviation of texture coefficient from the unity (*Tc*(002) of sample is 0.82 ≤ 1). The lattice parameters 'a' and 'c' are calculated using [26, 27]

$$\frac{1}{d_{hkl}^2} = \left(\frac{hk + {}^2 + {}^2}{3a^2}\right) + \frac{{}^2}{c^2}$$

The lattice parameter 'a' and 'c' values of ZnO nanorod composed films are given in Table 1.

3.3. Scanning electron microscopy (SEM)

The effect of PVA content on morphology of ZnO nanorods composed films is carried out using Scanning electron microscope (SEM) with energy dispersive analysis by X-rays (EDAX) attachment. Fig. 3(a) shows SEM image of the sample prepared at 180 °C, which is seen to be dark

brown and amorphous ZnO fine particles are uniformly stabilized in PVA matrix. The surface morphology of samples prepared without PVA displayed non homogeneous and randomly grown rods on the glass substrate as shown in Fig 3(b). The 0.5 and 1 Wt% PVA assisted grown films surface morphology showed the nanorods (Fig. 3(c&d)). Compared to 0.5 Wt%, 1 Wt% PVA assisted grown films are uniformly composed with large scale vertically oriented nanorods (Fig. 3(d)). With further increase of PVA content to 2 Wt%, length of the rods are decreased as shown in Fig. 3(e), higher

concentration of PVA restrict the growth of nanorods. This might be due to the addition of small amounts of PVA, which changes the viscosity of the aqueous solution to a large degree. The higher viscosity of the aqueous solution leads to the non uniform distribution of particles in PVA matrix. The energy dispersive x-ray spectrum of the 1 Wt% PVA assisted grown ZnO nanorod array film is shown in Fig. 3(f). The EDAX spectrum demonstrates that presence of Zn and O, which further confirmed that no other impurities in the ZnO host matrix.
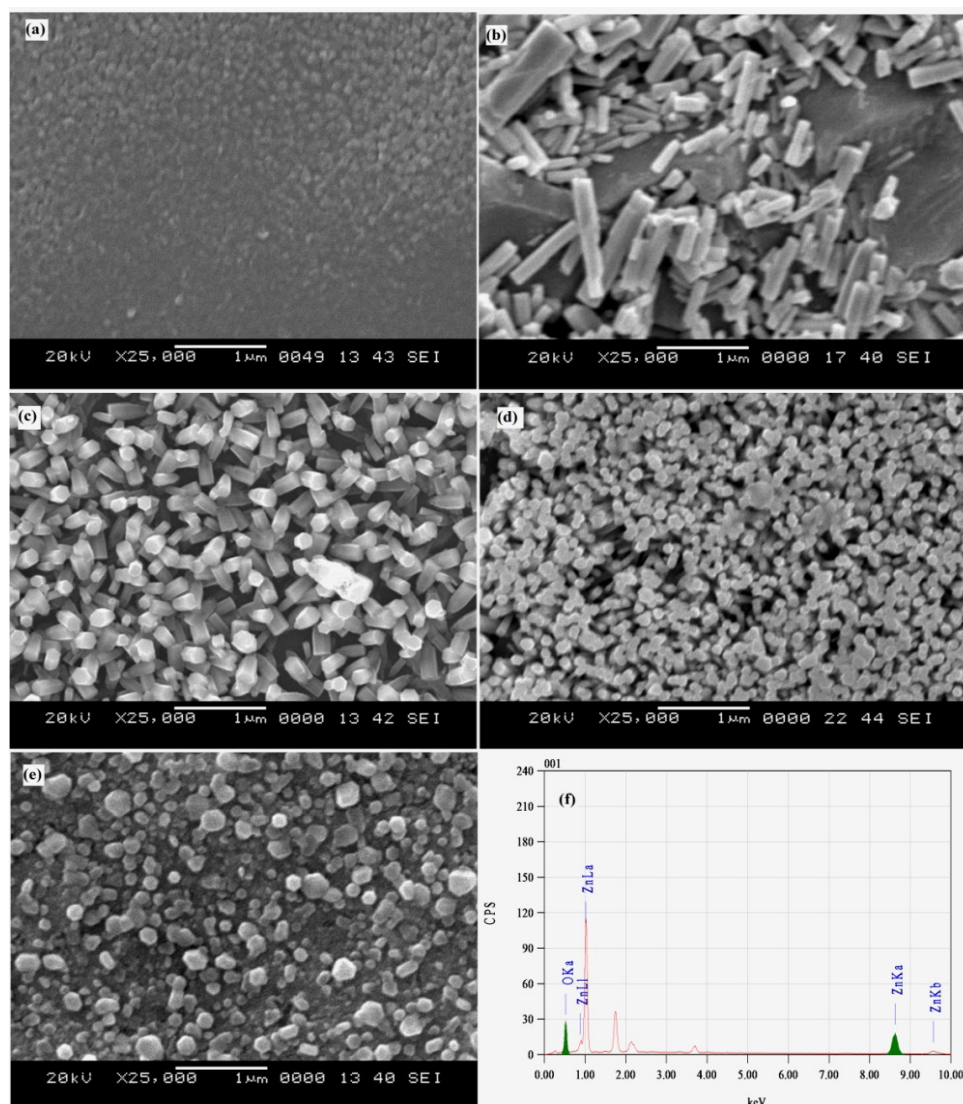

Fig. 3. SEM micrographs of ZnO films prepared in presence of different PVA content (a) 1 Wt% at 180°C, (b) 0 Wt% at 450°C, (c) 0.5 Wt% at 450°C, (d) 1 Wt% at 450°C, (e) 2 Wt% at 450°C, (f) EDX of ZnO.

3.4. Raman and photoluminescence study

Raman scattering is an effective characterisation technique to investigate the crystallization, structural disorder and defects in the nano and microstructures, vibration properties of as grown hexagonal shaped ZnO nanorods. ZnO with hexagonal wurtzite structure

belongs to the C_{6v}^4 space group. There are 4 atoms per unit cell leading to 12 phonon branches, nine optical phonon modes and three acoustic phonon modes, namely, three longitudinal-optical (LO) and six transverse-optical (TO) branches, one longitudinal-acoustic (LA), and two transverse-acoustic (TA).
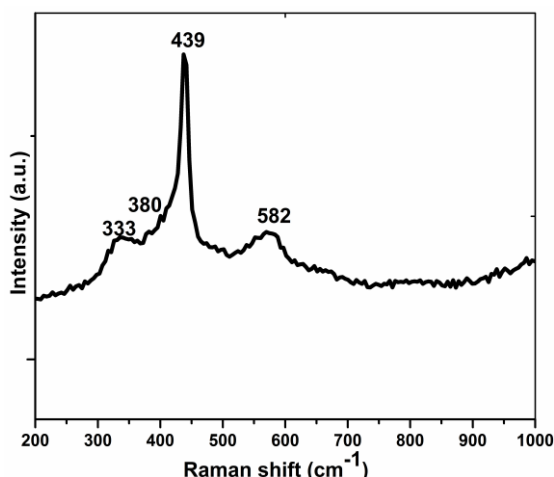
Fig. 4. Raman spectrum recorded on 1 Wt% PVA assisted grown ZnO nanorod array film.

Fig. 5. Photoluminescence spectrum recorded on 1 Wt% PVA assisted grown ZnO nanorod array film.

According to group theory, the optical phonons at the Γ point of the Brillouin zone [27].

$$\Gamma_{opt} = A_1 + 2B_1 + E_1 + 2E_2$$

Among these, A_1 and E_1 are polar modes and are both infrared and Raman active, whereas the B_1 modes are both infrared and Raman inactive (silent modes). The two non-polar E_2 modes (E_2(low) and E_2(high)) are only Raman active. Moreover, A_1 and E_1 modes can be split into transverse (TO) and longitudinal optical (LO) phonons due to the macroscopic electric fields associated with the LO phonons. Fig. 4 shows the typical room temperature Raman spectrum of the as-grown ZnO nanostructures. A sharp and dominant peak at 439 cm^{-1} can be assigned to the E_2(high) mode of non-polar optical phonons, which is the characteristic peak of the hexagonal wurtzite phase [28,29]. The peak at 380 cm^{-1} corresponds to A_1 transverse optical (TO) mode. A small and suppressed peak at 582 cm^{-1} attributed to E_1(LO) mode. Generally, the E_1(LO) mode is related to the structural defects (oxygen vacancies, zinc interstitials, free carriers, etc.) in ZnO [29,30]. In addition, the peak at 333 is due to multiple phonon (E_2(high)-E_2(low)) scattering processes [27]. Finally, the presence of an intense E2(high) mode and a suppressed E1(LO) mode in the Raman spectrum represents that the as-synthesized ZnO nanostructures are highly crystalline with a hexagonal wurtzite phase.

Fig. 5 shows the typical room-temperature photoluminescence (PL) spectra of the aligned hexagonal ZnO nanorod arrays grown by modified sol gel process. The spectra is recorded with excitation at 325 nm in the range 300-600 nm.

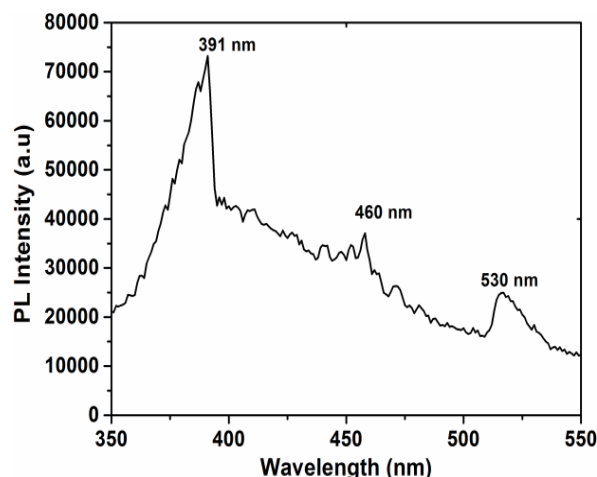Clearly, three emission bands have been observed from the room-temperature PL spectrum of the ZnO nanostructures, i.e., UV emission centered at 391 nm, blue emission centered at 460 nm and green emission centered at 530 nm, respectively. The UV emission is also called near band edge (NBE) emission, and it is generally originates from the direct recombination of free excitons through an exciton-exciton collision process [31]. Regarding the appearance of blue emission in ZnO nonmaterials, Gyan *et al.* reported that blue emission at 460 nm might be due to the transition from bottom of the conduction band to oxygen related defects namely oxygen vacancies or oxygen interstitials rather than deep level emission. Thus, we believe that the low intensity peaks for the blue emission bands appeared due to oxygen related intrinsic defects like oxygen interstitials and oxygen vacancies [32,33]. However, the exact mechanism behind this emission is still not clear. The green emission is also known to be a deep level emission (DLE), various explanations have been proposed for the origination of green emissions in the PL spectrum of ZnO nanostructures, it is generally caused by radial recombination of a photogenerated hole with electron of the singly ionized oxygen (O) vacancies in the surface lattices of the ZnO [31,33]. Moreover, it is also due to the radiative transitions between shallow donors (related to O vacancies) and deep acceptors (Zn vacancies) [33]. Interestingly, it is observed that, the ratio of I_{Uv}/I_{DLE} is found to be 1.65 and the UV emission is sharp and strong as compared to the blue and green emission bands. It has been reported that the high-crystallinity and perfection in surface states may enhance the UV emission in the PL spectrum [31, 33]. In our synthesized ZnO nanostructure arrays, the room temperature PL spectrum exhibit a strong and sharp UV emission, which confirms that the grown arrays have good optical properties with few structural defects such as oxygen vacancies and zinc.

3.5. Growth mechanism

In the present work we used PVA-citric acid gel to grow the nanorods on glass substrate. The primary factors affecting the growth of vertically oriented ZnO nanorods are the amount of the PVA, citric acid and the calcining temperature. Here we selected water soluble polyvinyl alcohol (PVA) as complex polymer and serves as a carrier. Moreover, it is acts as a spacer and promoter for zinc oxide nano rod growth [14]. PVA not only confines the growth units diameter, but also directs the one-dimensional orientation growth. Because of the existence of the citric acid, the surface tension of solution is reduced, which lower the energy needed to form a new phase of ZnO crystal. On the other hand, through two carboxyls and one hydroxyl, the citric acid and the zinc ion form two chelate rings, namely a pentabasic ring and a hexahydric ring [19, 34]. Because the occurrence of two chelate rings, the spatial volume of growing units is expanded. It has been known that the adsorption of growth units on crystal surfaces strongly affects the growth speed and orientation of crystals [34]. When the deposited films/precursors are calcined, the molecules of complex compound tend to be perpendicular to the absorbed surface and the growth units would tend to face land onto the growing interface. Since this kind of landing and dehydration will result in four Zn–O bonds, which make the face-landing of growing units on axial energetically preferable to both vertex and edge landing along the radial direction[19]. Because of the different growth rate of crystal plane, ZnO growth units further grow to hexagonal rod shape structure.

4. Conclusions

We have grown oriented ZnO arrays using the PVA-CA modified sol-gel process and studied the effect of PVA concentration. In the present study, PVA not only confined the growth units diameter, but also directed the one-dimensional orientation growth. The SEM and XRD studies suggested that PVA assisted grown ZnO films are composed of nanorods, with (002) preferred orientation. The size of the crystallite is reduced with the PVA concentration. The room temperature Raman spectrum exhibited strong peak at 437.8 cm^{-1} is one of the characteristic peaks of wurtzite ZnO. PL spectrum exhibited a strong and sharp UV emission at 391 nm, which confirms that the grown arrays have good optical properties with few structural defects. The main advantage of the proposed method is its simplicity and seed layer free. This simple approach should promise us a future large-scale preparation of ZnO nanorod arrays and other nonmaterials for many important applications in nanotechnology.

References

[1] M. H. Huang, S. Mao, H. Feick, H. Q. Yan, Y. Y. Wu, H. Kind, E. Weber, R. Russo, P. D. Yang, Science **292**, 1897 (2001).

[2] R. Könenkamp, R. C. Word, M. Godinez., Nano Lett. **5,** 2005 (2005).

[3] W. I. Park, G. C. Yi, Adv. Mater. **16,** 87 (2004).

[4] O. Lupan, V. M. Guérin, I. M. Tiginyanu, V. V. Ursaki, L. Chow, H. Heinrich, Th Pauporté, Journal of Photochemistry and Photobiology A: Chemistry **211**, 65 (2010).

[5] J. Y. Son, S. J. Lim, J. H. Cho, W. K. Seong, H. Kim, Appl. Phys. Lett., **93**, 053109 (2008).

[6] X. Wang, C. J. Summers, Z. L. Wang, Nano Lett. **4,** 423 **(**2004).

[7] Z. Guang, Y. Zhou, S. Wang, R. Yang, Y. Ding, X. Wang, Y. Bando, Z.Wang, Nanotechnology **23**, 055604 (2012).

[8] P. C. Chang, Z. Fan, D. Wang, W. A. Tseng, J. H. Chiou, J. G. Lu, Chem. Mater. **16**, 5133 (2004).

[9] W. I. Park, D. H. Kim, S. W. Jung, G. C. Yi, Appl. Phys. Lett. **80,** 4232 (2002).

[10] S. Baruah, J. Dutta, J Sol-Gel Sci Technol **50**, 456 (2009).

[11] M. Sima, I. Enculescu, M. Sima, M. Enache, E. Vasile, J. P. Ansermet, Phys. Status Solidi B **244**, 1522 (2007).

[12] B. B. Lakshmi, P. K. Dorhout, C. R. Martin, Chem. Mater. **9**, 857 (1997).

[13] N. Huang, M. W. Zhu, L. J. Gao, J. Gong, C. Sun, X. Jiang, Appl. Surf. Sci. **257**, 6026 (2011).

[14] W. Sang, Y. Fang, J. Fan, Y. He, J. Min, Y. Qian, J. Cryst. Growth 299, **272** (2007).

[15] Y. C. Chang, L. J. Chen, J. Phys. Chem. C **111**, 1268 (2007).

[16] Z. Liu, L. E. J. Ya, Y. Xin. Appl. Surf. Sci. **255**, 6415 (2009).

[17] P. B. Renee, C. L. Fields, B. A. Gregg, Langmuir **20**, 5114 (2004).

[18] Y. Tak, K. Yong, J. Phys. Chem. B **109,** 19263 (2005).

[19] Z. Yang, Q. H. Liu, H. C. Yu, B. Zou, Y. G. Wang, T. H. Wang, Nanotechnology **19**, 035704 (2009).

[20] D. S. Boyle, K. Govender, P. O'Brien, Chem. Commun. **1**, 80 (2002).

[21] X. D. Gao, X. M. Li, W. D. Yu, L. Li, J. J. Qiu, Appl. Surf. Sci. **253**, 4060 (2007).

[22] R. Kaur, A. V. Singh, K. Sehrawat, N. C. Mehra, R. M. Mehra, J. Non-Cryst. Solids **352**, 2565 (2006).

[23] S. Ilican, Y. Caglar, M. Caglar, F. Yakuphanoglu, Appl. Surf. Sci. **255**, 2353 (2008).

[24] Y. Nishio, R. S. Manley, Macromolecules **21**, 1270 (1988).

[25] A. Santhosh Kumar, K. K. Nagaraja, H.S. Nagaraja. J Mater Sci: Mater Electron **24**, 3812 (2013).

[26] B. D. Cullity, S. R. Stock, Elements of X-ray Diffraction, Prentice Hall, New Jersey 619 (2001).

[27] O. Lupan, L. Chow, L. K. Ono, B. R. Cuenya, G. Chai, H. Khallaf, S. Park, A. Schulte, J. Phys. Chem. C **114**, 12401 (2010).

[28] A. Umar, B. K. Kim, J. J. Kim, Y. B. Hahn, Nanotechnology **18**, 175606 (2007).

[29] Z. Peng, G. Dai, W. Zhou, P. Chen, Q. Wan, Q. Zhang, B. Zou, Appl. Surf. Sci. **256**, 6814 (2010).

[30] A. Umar, S. H. Kim, H. Lee, N. Lee, Y. B. Hahn, J. Phys. D: Appl. Phys. **41**, 065412 (2008).

[31] A. Umar, Y. B. Hahn, Nanotechnology **17**, 2174 (2006).

[32] R. N. Gayen, K. Sarkar, S. Hussain, R. Bhar, A. K. Pal, Indian J. Pure Appl. Phys. **49,** 470 (2011).

[33] A. Umar, C. Ribeiro, A. Al-Hajry, Y. Masuda, Y. B. Hahn, J. Phys. Chem. C, **113**, 14715 (2009).

[34] Z. Yang, Q. H. Liu, L. Yang, Mater. Res. Bull. **42**, 221 (2007).

---

[*]Corresponding author: saanthosh.phy@gmail.com, hosakoppa@gmail.com.